LRP 636/99 June 1999

Magnetic topology and guiding center drift orbits in a reversed shear tokamak

O. Fischer, W.A. Cooper, L. Villard

submitted for publication to
Nuclear Fusion

ISSN 0458-5895

Magnetic Topology and Guiding Center Drift Orbits in a Reversed Shear Tokamak

O. Fischer*, W.A. Cooper, L. Villard
Centre de Recherches en Physique des Plasmas, Association Euratom-Confédération Suisse, Ecole Polytechnique Fédérale de Lausanne, CRPP-PPB,CH-1015 Lausanne, Switzerland

June 8, 1999

*E-mail: Olivier.Fischer@epfl.ch

Abstract

The magnetic topology and particle drift orbits are analyzed in a monotonic q profile and in a reversed shear TEXTOR equilibrium that is subject to a magnetic perturbation driven by the Dynamic Ergodic Divertor (DED). The main results prove that there exists a transport barrier for the magnetic field lines and for circulating particles in the reversed shear case when the DED is applied. This transport barrier occurs near the surface of minimum q value where the KAM theory may be invalid. Moreover, we have remarked that trapped particles are lost due to the presence of the ripple and the DED does not affect their trajectories. To analyze the magnetic topology, we use a symplectic perturbed map and the guiding center orbits are evaluated in the Boozer coordinates.

1 Introduction

We have studied the magnetic topology and the guiding center drift orbits in a TEXTOR Tokamak with the Dynamic Ergodic Divertor (DED) [1]. The study has been done with two different equilibria computed with the 3D free boundary VMEC code. The 3D behavior is not due to the DED, because we treat it as a magnetic perturbation and we do not include it for the achievement of equilibria. On the other hand, we take into account the ripple due to the discrete number of toroidal coils. The first equilibrium is computed by imposing a monotonic profile for the safety factor contrary to the second one which is a reversed shear configuration. In fact, we are interested in investigating the difference between these two equilibria subject to the DED and to compare the difference between the magnetic topology and the particle drifts.

The fact that the system studied is governed by the KAM (Kolmogorov, Arnold and Moser) theory (magnetic islands on resonant surfaces, KAM barriers, etc.) [2], we expect that in a reversed shear system the physics should be totally different from the monotonic case. Actually, the KAM theorem assumes that the profile of the safety factor must be a monotonic function. Some results [3] show that in a reversed shear there exists a strong transport barrier. So the study of the magnetic field lines yields information concerning the magnetic properties and the trajectories of particles too. To analyze the magnetic topology, we use a symplectic perturbed map [4] which allows us to study the statistical properties of the topology. In particular, we can evaluate a local diffusion coefficient for the magnetic field lines.

Of course, to complete the analysis, we have to consider the behavior of particles. The most common way is to use a guiding center drift theory in Boozer coordinates [5, 6, 7, 8]. We have developed a code which is able to solve the equations of the guiding center orbits in the presence of a radial magnetic perturbation. To obtain good statistical properties, we have to solve these equations for approximatively 10^4 particles. To realize it, we run the program on a massively parallel computer. For the simulations, we have put 80×10^3 Deuterium particles and follow them during 10 $[ms]$ in one hour and half CPU time. With this code, we can compare the results of the drift orbits with the magnetic topology. What we have found is that in a reversed shear case, a transport barrier occurs for circulating particles when the DED is applied. Furthermore, only the circulating particles are affected by the DED contrary to the trapped particles which are lost only by the effect of the ripple.

With respect to the organization of the paper, we first review the theory

of the mapping procedure for the magnetic topology and the guiding center drift orbits in Boozer coordinates are described. Then, we will discuss the results for a monotonic case profile TEXTOR equilibrium with and without the DED and compare these results with a reversed shear configuration. Finally a discussion of the main results will be summarized in the conclusion.

2 Review of the Theory

2.1 The mapping procedure

The study of the magnetic topology is done by using a symplectic perturbed map [4]. In fact, if we examine the intersections of the trajectory with a $\varphi = constant$ cross section (φ is the geometric toroidal angle), we can define a map:

$$\begin{cases} J_{n+1} &= J_n + \epsilon f(J_{n+1}, \theta_n) \\ \theta_{n+1} &= \theta_n + 2\pi/L\iota(J_{n+1}) + \epsilon g(J_{n+1}, \theta_n),\ mod(2\pi), \end{cases} \tag{1}$$

where $f = -\int_0^{2\pi/L} d\varphi \frac{\partial \chi}{\partial \theta}$ and $g = -\int_0^{\theta} d\theta' \frac{\partial f}{\partial J}$ are the contributions of the magnetic perturbation, ι is the rational transform, ϵ is the amplitude of the perturbation and L the periodicity of the system. The J coordinate is proportional to the toroidal flux function and can be considered to a radial coordinate, θ is a poloidal angle in which the magnetic field lines are straight [9, 10]. Finally, χ is the contribution of the magnetic perturbation and it is proportional to the poloidal flux function. In this case, the total poloidal flux function can be written as a contribution due to the equilibrium given by the VMEC code plus a magnetic perturbation:

$$\chi_{tot} = \underbrace{\chi_0(J)}_{equilibrium} + \underbrace{\chi(J, \theta, \varphi)}_{DED}.$$

By using equation (1), we can analyze the statistical properties of the system, especially, we can compute a local diffusion coefficient for field lines. In fact for a open mixed system, we can assume that the probability of the radial transition is given by a Gaussian distribution $P(J, J_o, n) \sim \frac{1}{\sqrt{4\pi D(J_0) n}} \exp -\frac{(J-J_0)^2}{4D(J_0)}$ [11] when the number of iterations is small. The fact is that for small values of n, the magnetic field lines can neither see the openness of the system nor the KAM barriers and so the diffusion must be a normal diffusive process. Consequently, the local diffusion coefficient $D(J_o)$ can be estimated by $D(J_0) \sim \frac{<(J(n)-J_0)^2>}{2n}$, where the average is done over an ensemble of initial conditions. For large n, the probability distribution ceases to be Gaussian.

2.2 The guiding center drift orbit

The guiding center drift orbit theory has been described in [5, 7, 8]. In this paper, we employ the notation of [6]. As mentioned in [5, 6], we use a

relativistic guiding center theory in Boozer coordinates (s, ϑ, ξ) where $s = \psi/\psi(s=1)$ is a radial coordinates, ϑ and ξ are a poloidal and toroidal angle, respectively. The magnetic equilibrium field is given by $\mathbf{B} = \nabla\psi \times \nabla\vartheta + \nabla\xi \times \nabla\chi$ in the contravariant representation and $\mathbf{B} = B_s\nabla s + \mu_o J(s)\nabla\vartheta - \mu_o I(s)\nabla\xi$ in the covariant form. $\psi(s)$ and $\chi(s)$ are the toroidal and poloidal flux functions, respectively, and $2\pi I(s)$ and $2\pi J(s)$ are the poloidal and toroidal current fluxes.

The Boozer magnetic coordinates are canonical for perturbed magnetic fields that satisfy the condition $\delta\mathbf{B} = \nabla\times\big(\Upsilon(s,\vartheta,\xi)\mathbf{B}\big)$ [5, 7, 8]. We therefore relate the radial component of the perturbation of the DED coils to the scalar function $\Upsilon(s,\vartheta,\xi)$ by

$$\delta\mathbf{B}\cdot\nabla s = -\frac{\mu_o}{\sqrt{g}}\Big(I(s)\frac{\partial\Upsilon}{\partial\vartheta} + J(s)\frac{\partial\Upsilon}{\partial\xi}\Big), \tag{2}$$

where $(\sqrt{g})^{-1} = \nabla s\times\nabla\vartheta\cdot\nabla\xi$ is the Jacobian of the transformation and $\delta\mathbf{B}$ is the magnetic field of the DED computed with the Biot-Savart law. If we assume that

$$\Upsilon(s,\vartheta,\xi) = \sum_{m,n}\Upsilon^c_{mn}(s)\cos(m\vartheta - nL\xi) + \Upsilon^s_{mn}(s)\sin(m\vartheta - nL\xi),$$

equation (2) gives

$$\Upsilon^c_{mn}(s) = \frac{\delta^s_{mn}(s)}{\mu_o\big[mI(s) - nLJ(s)\big]},\ \text{for } m,n\neq 0$$

$$\Upsilon^s_{mn}(s) = \frac{\delta^c_{mn}(s)}{\mu_o\big[nLJ(s) - mI(s)\big]},\ \text{for } m,n\neq 0$$

$$\Upsilon^c_{0,0}(s) = \Upsilon^s_{0,0}(s) = 0$$

where

$$\delta^{c,s}_{mn}(s) = 2L/(2\pi)^2\int_o^{2\pi}d\vartheta\int_o^{2\pi/L}d\xi\sqrt{g}\delta\mathbf{B}\cdot\nabla s\begin{cases}\cos(m\vartheta - nL\xi)\\ \sin(m\vartheta - nL\xi)\end{cases}$$

and L is the periodicity of the system.

By introducing e and m_o the electronic charge and the rest mass of the particle, γ the relativistic gamma factor, μ the magnetic moment and

$\rho_{\|} = p_{\|}/(eB)$, the equations of the relativistic guiding center are given by [5, 6, 8]

$$\dot{s} = \frac{\mu_o I(s)}{D}\Big[\frac{1}{\gamma}\big(\frac{\mu}{e} + \frac{eB}{m_o}\rho_{\|}^2\big)\frac{\partial B}{\partial \vartheta} - \frac{eB^2\rho_{\|}}{\gamma m_o}\frac{\partial \Upsilon}{\partial \vartheta}\Big]$$

$$+\frac{\mu_o J(s)}{D}\Big[\frac{1}{\gamma}\big(\frac{\mu}{e} + \frac{eB}{m_o}\rho_{\|}^2\big)\frac{\partial B}{\partial \xi} - \frac{eB^2\rho_{\|}}{\gamma m_o}\frac{\partial \Upsilon}{\partial \xi}\Big], \tag{3}$$

$$\dot{\vartheta} = \frac{eB^2\rho_{\|}}{\gamma m_o D}\Big[\chi'(s) + (\rho_{\|} + \Upsilon)\mu_o I'(s) + \mu_o I(s)\frac{\partial \Upsilon}{\partial s}\Big]$$

$$-\frac{\mu_o I(s)}{D}\frac{1}{\gamma}\big(\frac{\mu}{e} + \frac{eB}{m_o}\rho_{\|}^2\big)\frac{\partial B}{\partial s}, \tag{4}$$

$$\dot{\xi} = \frac{eB^2\rho_{\|}}{\gamma m_o D}\Big[\psi'(s) + (\rho_{\|} + \Upsilon)\mu_o J'(s) + \mu_o J(s)\frac{\partial \Upsilon}{\partial s}\Big]$$

$$-\frac{\mu_o J(s)}{D}\frac{1}{\gamma}\big(\frac{\mu}{e} + \frac{eB}{m_o}\rho_{\|}^2\big)\frac{\partial B}{\partial s}, \tag{5}$$

$$\dot{\rho}_{\|} = -\frac{1}{D}\Big[\chi'(s) + (\rho_{\|} + \Upsilon)\mu_o I'(s) + \mu_o I(s)\frac{\partial \Upsilon}{\partial s}\Big]\frac{1}{\gamma}\big(\frac{\mu}{e} + \frac{eB}{m_o}\rho_{\|}^2\big)\frac{\partial B}{\partial \vartheta}$$

$$-\frac{1}{D}\Big[\psi'(s) + (\rho_{\|} + \Upsilon)\mu_o J'(s) + \mu_o J(s)\frac{\partial \Upsilon}{\partial s}\Big]\frac{1}{\gamma}\big(\frac{\mu}{e} + \frac{eB}{m_o}\rho_{\|}^2\big)\frac{\partial B}{\partial \xi}$$

$$+\frac{\mu_o}{D}\Big[I(s)\frac{\partial \Upsilon}{\partial \vartheta} + J(s)\frac{\partial \Upsilon}{\partial \xi}\Big]\frac{1}{\gamma}\big(\frac{\mu}{e} + \frac{eB}{m_o}\rho_{\|}^2\big)\frac{\partial B}{\partial s}, \tag{6}$$

where

$$D = \mu_o\Big[\chi'(s)J(s) - \psi'(s)I(s)\Big]\Big[1 + \mu_o(\rho_{\|} + \Upsilon)\frac{J(s)I'(s) - I(s)J'(s)}{\chi'(s)J(s) - \psi'(s)I(s)}\Big].$$

For the integration of equations (3), (4), (5) and (6), we use a fourth order Runge-Kutta scheme with fixed time step. The time step is chosen in such a way that the solution gives similar results by using a variable order, variable

step size given by the NAG D02CJF library [12] and a fourth order Runge-Kutta symplectic integrator [13]. Typically, the time step is approximatively 4×10^{-7} $[s]$ for all the simulations. Finally, to minimize the time of the simulation, we have parallelized the algorithm. The parallelization consists in having a master processor which gives initial conditions to slave processors which resolve the equations (3), (4), (5) and (6). With this method, we can follow up to 10^4 Deuterium particles during 10 $[ms]$ in one hour and half CPU time by using sixteen processors. Concerning the initial conditions, we choose (s, ϑ, ξ) and the pitch angle randomly. The energy of the particle is determined by the profile $E_c(s) = 500(1 - s^2) + 100$ $[keV]$. Finally, all the quantities appearing in equations (3), (4), (5) and (6) are stored on a 3D array of dimension $(100 \times 80 \times 80)$ in the (s, ϑ, ξ) direction.

3 Numerical Results

The first part of the results concentrates on analyzing the effect of the Dynamic Ergodic Divertor (DED) [1] in a TEXTOR Tokamak equilibrium with a monotonic safety factor profile. The equilibrium is computed using the 3D free boundary VMEC code taking in account the ripple due to the discrete number of toroidal coils (less than 1 %). The TEXTOR Tokamak is composed of sixteen toroidal coils and two vertical field coils. The plasma current is approximatively 350 $[kA]$ and the value of q at the edge of the plasma is 3.4 (Fig. 1a). The second part consists to achieve a reversed shear configuration and to analyze the difference with the monotonic case. The parameters of the reversed shear equilibrium are comparable to those of the standard shear case, but the shear is different and the minimum q value is localized at $s \sim 0.8$ (Fig. 1a). Finally, the DED is composed of eighteen helical coils, two of which are compensation coils, inside the vacuum vessel on the high field side (HFS) and they are aligned to coincide with the pitch of the field lines on the $q = 3$ rational surface. We model the current in the coils by

$$I_j = cc \times I_o \sin((j-1)\pi/2 + \Omega t),\ j = 1, 16,\ I_o = 15\,[kA],\ \Omega t = \pi/4$$

and for the compensation coils $I_c = \pm cc \times I_o/\sqrt{2}\sin(5\pi/4 + \Omega t)$. As we note, the magnetic perturbation is assumed to be "quasi-static" and the periodicity of the system is $L = 4$. The parameter cc corresponds to the amplitude of the current in the DED.

3.1 Properties of the magnetic topology

The first analysis consists to study the Poincaré cross section. As the system is a Hamiltonian system subjected to a weak perturbation, the KAM (Kolmogorov Arnold and Moser) [2] theory is applicable. It demonstrates that on the resonant surfaces (q is a rational number) magnetic islands appear. On non-resonant surfaces, however, KAM barriers still exist. But the KAM theory assumes that the rational transform must be a monotonic function, $|\iota'(s)| = |(1/q(s))'| > 0$, otherwise the KAM theorem cannot be demonstrated. By taking a reversed shear configuration, we expect to have a different behavior for the magnetic field line topology because a transport barrier will occur [3] near the surface for which $\iota'(s) = 0$. Another difference is the separatrix reconnection near this surface. In fact, near this surface, there exists two identical chains of magnetic islands separated by a KAM barrier if the perturbation is weak. By increasing it, the width of islands will

grow and at a certain value for the perturbation, the two chains should overlap. But contrary to a monotonic case, this overlap does not create chaos but a bifurcation occurs and this is referred to as a separatrix reconnection [3]. From the point of view of the topology, the separatrix reconnection is the bifurcation from a heteroclinical topology to a homoclic topology.

In Fig. 1b), we show the Poincaré cross section for the monotonic q profile equilibrium with an amplitude $cc = 0.8$ for the DED. Clearly, we see magnetic island structures on the $q = 10/4$, $q = 11/4$ ($J/J_{max} \sim .72$ and 0.8 respectively) surfaces and a large part of the magnetic field is stochastic between these two chains. Now if we regard, for the same amplitude of the DED, the Poincaré cross section for the reversed shear case in Fig. 1c), we see clearly that a transport barrier occurs near the value $J/J_{max} \sim s \sim 0.83$. This is due to the fact that the q value has its minimum near this surface. Moreover, we expect that this barrier will change the local diffusion coefficient. By comparing Figs. 2a) and 2b), we see that for the reversed shear equilibrium the amplitude of the local diffusion coefficient is six times smaller than for the monotonic case. But we do not observe any transport barriers in the profile of D, because by definition of the local diffusion coefficient, D does neither take in account any KAM barriers nor transport barriers (section 2.1). But by analyzing the probability of transition $P(J, J_o, n)$, we can observe a transport barrier, because $P(J, J_o, n)$ can be evaluated at large iteration number n (section 2.1). In Fig. 2c), we plot $P(J, J_o, n)$ after 25×10^3 iterations for the reversed shear case and the amplitude of the DED is $cc = 0.8$. Clearly, we observe a transport barrier near $s \sim 0.83$ which corresponds approximatively to the minimum q value.

3.2 Guiding center drift orbits

With respect to the behavior of particles, we study the percentage of lost particles with and without the DED. Firstly, if we analyze the case of the monotonic safety factor without the effect of the DED, we expect that only the trapped particles should leave the plasma. Fig. 3a) shows the percentage of lost particles as a function of time. The circles represents the total number of particles lost divided by the total number of particles (80×10^3), the crosses and the squares are the total number of trapped and circulating particles lost, respectively, divided by the total number of particles and the stars (triangles) are the total number of trapped (circulating) particles lost divided by the total trapped (circulating) particles. Clearly, only the trapped particles leave the plasma contrary to the circulating particles which are confined within the plasma and the total lost particle fraction is

approximatively 4%. Concerning the distribution of lost particles in a (ξ, ϑ) cross section, we see in Fig. 3b) that the trapped particles leave the plasma where the rippled B field strength reaches a minimum betwenn the sixteen toroidal coils locations. The fact that we lose the trapped particles only for $0 < \vartheta < \pi$ is due to the $\mathbf{B} \times \nabla B$ drift. Actually, by changing the sign of particles, we change the ϑ position, i.e. we lose particles for $\pi < \vartheta < 2\pi$. Finally, in Fig. 3c) we plot the particles lost as a function of their initial positions and we see that the profile of lost trapped particles increases when s_{init} approaches the boundary of the plasma.

By switching on the DED, we expect that only the circulating particles should see the DED, because the DED is localized to the HFS. So the trapped particles which are by definition localized on the low field side (LFS), are not affected by the presence of the DED coils in contrast to the circulating particles [14]. Fig 4a) shows the behavior of particles lost as a function of time and clearly the percentage of the total particles lost increases by a factor 3 compared with Fig. 3a). This increase is due to the fact that we lose many more circulating particles while the trapped particles lost are not modified significantly compared with Fig. 3a). Moreover by looking at Fig. 3b), we can observe that the circulating particles leave the plasma near the region of the DED ($2 < \vartheta < 4$) and the structure of oblique lines is caused by the geometry of the coils of the DED. Finally in Fig. 4c), we see that circulating particles for which the initial radial position is greater than 0.8 are lost. Furthermore, there exists a maximum of percentage of lost particles at $s_{init} \sim 0.9$.

Now if we impose a reversed shear configuration, we expect that by switching off the DED all the statistical properties should be similar to the monotonic case. In fact, we have found that all quantities are of the same order. But by switching on the DED, we think that the behavior should change, because the study of the magnetic field lines shows a transport barrier. By comparing Figs. 4a) and 5a), we observe that in the reversed shear case the percentage of circulating particles lost decreases by a factor of six compared with the monotonic case. We can interpret this phenomena as the development of a transport barrier for circulating particles. We speculate that the trapped particles do not sense this barrier because the width of the banana orbit may be greater than the barrier width. This reduction of lost circulating particles is visible in Fig. 5b) too. Finally, by looking at Fig. 5c), we see clearly that there exists two different regions for the circulating particles. All circulating particles with initial radial positions that are smaller than 0.88 are confined, while those with $s_{init} > 0.88$ begin to drift out of the plasma. This separation of region describes a transport barrier

and the global behavior inside the barrier is totally different than outside [15]. The localization of this transport barrier coincides approximatively with the transport barrier of the magnetic field lines.

4 Conclusion

This work has shown the importance of the q profile in an equilibrium subject to a magnetic perturbation. The comparison between the magnetic topology and the drift particles has allowed to observe a strong relationship between magnetic field lines and the drift orbits. The main result of this paper demonstrates that only the circulating particles are affected by the presence of the DED. In comparison, the trapped particles are lost by the effect of the toroidal magnetic field ripple. In a reversed shear configuration, a transport barrier occurs for the magnetic field lines and in this case the local diffusion coefficient is reduced by a factor six.

The particle trajectories are qualitatively the same for configurations with and without reversed magnetic shear in the absence of magnetic field perturbations driven by the DED coils. When the DED is activated, a fraction of the otherwise very well confined circulating particles are lost. However, the percentage of circulating particles lost in the reversed shear case is a factor of four smaller than in the standard shear case. This indicates that the circulating particles may experience a transport barrier similar to that of the field lines that may be linked to the inapplicability of the KAM theory in the presence of a non-monotonic q profile. Consequently, the magnetic topology appears to play a predominant role in the transport barrier formation. We believe that the transport barrier for the particles is a consequence of the transport barrier of the magnetic field lines.

Finally, as we have seen, a transport barrier occurs when we have applied to the equilibrium a magnetic perturbation driven by the DED. Consequently, we could expect that either external magnetic fields such as error fields or internal instabilities constitute a perturbation to the equilibrium and could produce a transport barrier if the equilibrium has reversed shear. But this is still an open question in the physics of magnetically confined plasma systems.

ACKNOWLEDGMENTS

We thank Dr. S.P. Hirshman for providing us with the VMEC code and Dr. K.H. Finken and Dr. A. Nicolai for the input of the DED. This work was partially sponsored by the Fonds National Suisse de la Recherche Scientifique and by Euratom.

References

[1] Finken K. H. (Ed), The Dynamic Ergodic Divertor (DED) for TEXTOR, Rep. Jül-3285, Kernforschungszentrum Jülich (1996).

[2] Lichtenberg A. J., Lieberman M. A., Applied mathematical sciences **38** (New York: Springer-Verlag) (1992).

[3] del-Castillo D., Greene J. M. and Morrison P. J., Physica D **91** (1996) 1.

[4] Fischer O., Cooper W. A., Plasma Physics Reports **24** (1998) 784.

[5] Boozer A. H., Phys. Fluids **23** (1980) 904.

[6] Cooper W. A., Plasma Phys. Control. Fusion **39** (1997) 931.

[7] White R. B., Boozer A. H. and Hay R., Phys. Fluids **25** (1982) 575.

[8] White R. B., Chance M. S., Phys. Fluids **27** (1984) 2455.

[9] Fischer O., Cooper W. A., Plasma Phys. Control. Fusion **40** (1998) 1269.

[10] D'Haeseleer W. D., et al., Flux Coordinates and Magnetic Field Structure (New York: Springer-Verlag) (1991).

[11] Abdullaev S. S., Finken K. H. and Kaleck A., Phys. Plasmas **5** (1998) 196.

[12] Numerical Algorithms Group Fortran Library, Mark 15, The Numerical Algorithms Group Limited, Oxford (1991).

[13] Sanz-Serna J. M. and Calvo M. P., Applied Mathematics and Mathematical Computation **7** (London: Chapman & Hall) (1994).

[14] Montvai A., Fusion Enginnering and Design **37** (1997) 427.

[15] del-Castillo D., Dynamics and Transport in Rotating Fluids and Transition to Chaos in Area Preserving Nontwist Maps PH.D. thesis, Univ. of Texas at Austin (1994).

CAPTIONS

1. a) Profile of the safety factor q for the monotonic case (solid line) and for the reversed shear configuration (dot line) (top). b) Poincaré cross section for the monotonic q profile with $cc = 0.8$ (bottom left) and c) for the reversed shear profile with $cc = 0.8$ (bottom right).

2. Profile of the local diffusion coefficient as a function of the radial coordinate J/J_{max} for different values of cc. a) For the monotonic q profile (top left) and b) for the reversed shear profile (top right) (Crosses: $cc = 0.4$. Circles: $cc = 0.6$. Stars: $cc = 0.8$. Triangles: $cc = 1.0$). c) Probability of the radial transition $P(J, n)$ after 25×10^3 iterations for the reversed shear case and $cc = 0.8$. The initial conditions are $P(J, 0) = \delta(J - 0.775)$ (bottom).

3. Percentage of particles lost for the monotonic q profile without the DED a) as a function of time (Circles: $n_{tot}/ntot$. Crosses: $n_{tra}/ntot$. Squares: $n_{cir}/ntot$. Stars: $n_{tra}/ntra$. Triangles: $n_{cir}/ncir$) (top left). b) As a function of the poloidal and toroidal angles for the total lost particles (top right). c) As a function of the initial radial coordinate $0.3 \leq s_{init} \leq 0.95$ (Circles: $n_{tot}/ntot$. Crosses: $n_{tra}/ntot$. Squares: $n_{cir}/ntot$. Stars: $n_{tra}/ntra$. Triangles: $n_{cir}/ncir$) (bottom).

4. Percentage of particles lost for the monotonic q profile with $cc = 0.8$ a) as a function of time (Circles: $n_{tot}/ntot$. Crosses: $n_{tra}/ntot$. Squares: $n_{cir}/ntot$. Stars: $n_{tra}/ntra$. Triangles: $n_{cir}/ncir$) (top left). b) As a function of the poloidal and toroidal angles for the total lost particles (top right). c) As a function of the initial radial coordinate $0.8 \leq s_{init} \leq 0.98$ (Circles: $n_{tot}/ntot$. Crosses: $n_{tra}/ntot$. Squares: $n_{cir}/ntot$. Stars: $n_{tra}/ntra$. Triangles: $n_{cir}/ncir$) (bottom).

5. Percentage of lost particles for the reversed shear profile with $cc = 0.8$ a) as a function of time (Circles: $n_{tot}/ntot$. Crosses: $n_{tra}/ntot$. Squares: $n_{cir}/ntot$. Stars: $n_{tra}/ntra$. Triangles: $n_{cir}/ncir$) (top left).b) As a function of the poloidal and toroidal angles for the total lost particles (top right). c) As a function of the initial radial coordinate $0.8 \leq s_{init} \leq 0.98$ (Circles: $n_{tot}/ntot$. Crosses: $n_{tra}/ntot$. Squares: $n_{cir}/ntot$. Stars: $n_{tra}/ntra$. Triangles: $n_{cir}/ncir$) (bottom).

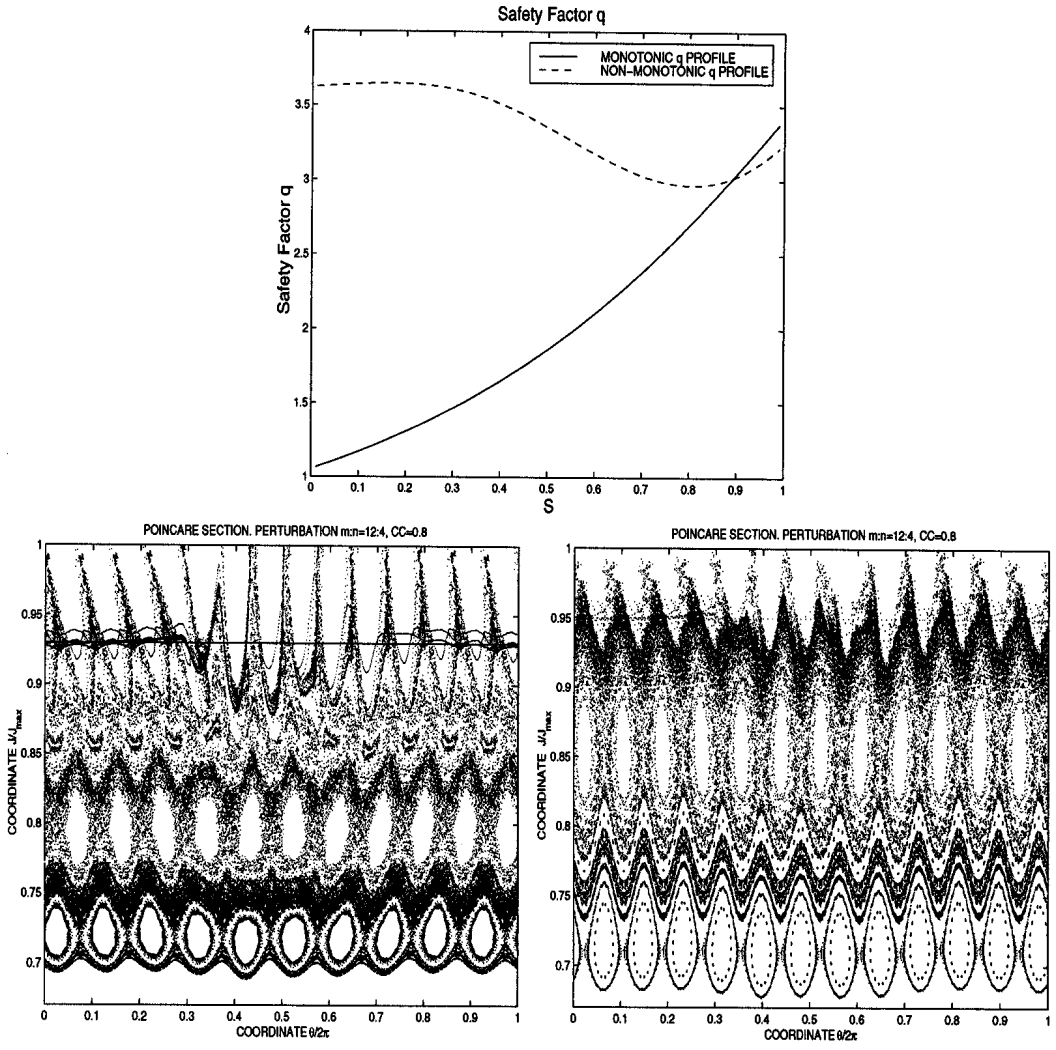
Safety Factor q
MONOTONIC q PROFILE
NON-MONOTONIC q PROFILE
Safety Factor q
S
POINCARE SECTION. PERTURBATION m:n=12:4, CC=0.8
COORDINATE J/J_max
COORDINATE θ/2π
POINCARE SECTION. PERTURBATION m:n=12:4, CC=0.8
COORDINATE J/J_max
COORDINATE θ/2π

Figure 1:

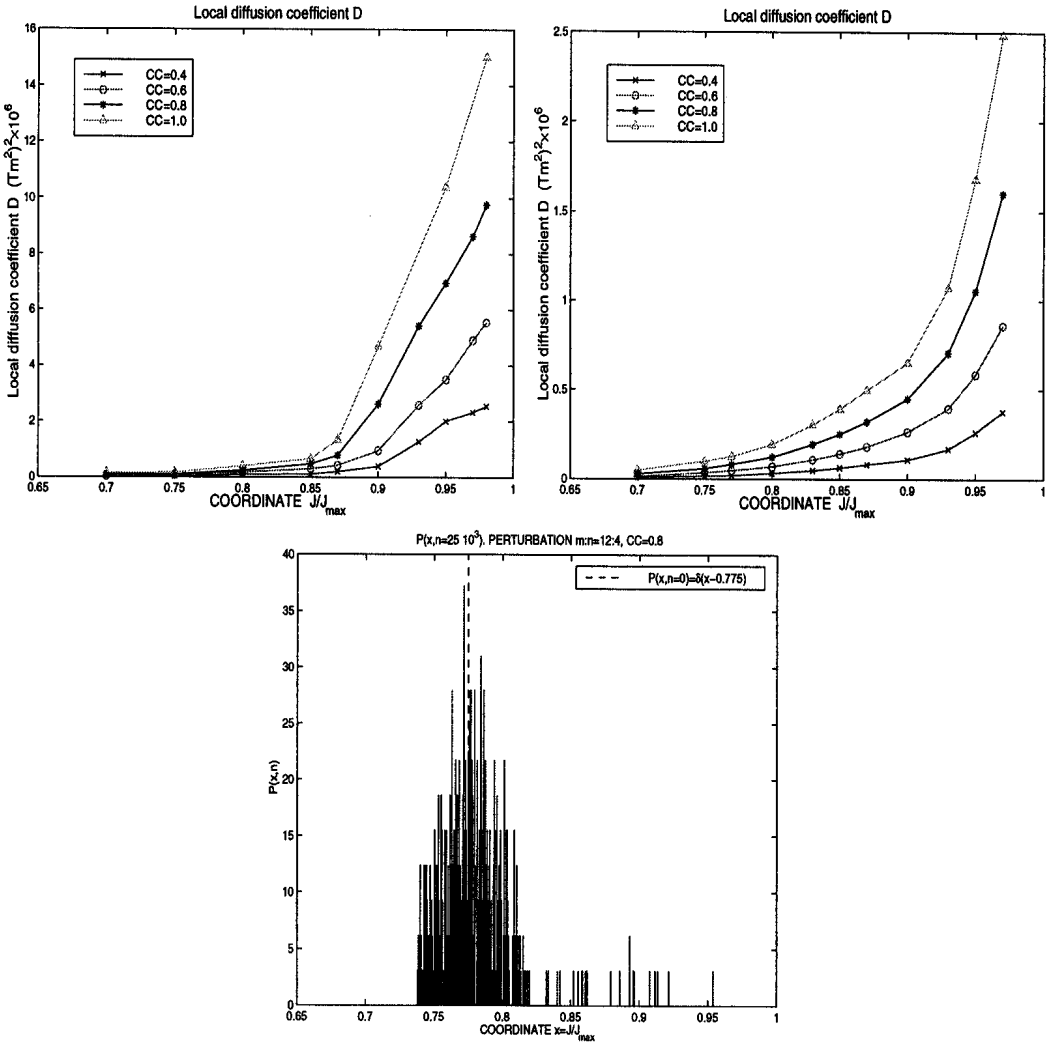
Local diffusion coefficient D
Local diffusion coefficient D (Tm²)²×10⁶
COORDINATE J/J_max
CC=0.4
CC=0.6
CC=0.8
CC=1.0
Local diffusion coefficient D
Local diffusion coefficient D (Tm²)²×10⁶
COORDINATE J/J_max
CC=0.4
CC=0.6
CC=0.8
CC=1.0
P(x,n=25 10³), PERTURBATION m:n=12:4, CC=0.8
P(x,n=0)=δ(x−0.775)
P(x,n)
COORDINATE x=J/J_max

Figure 2:

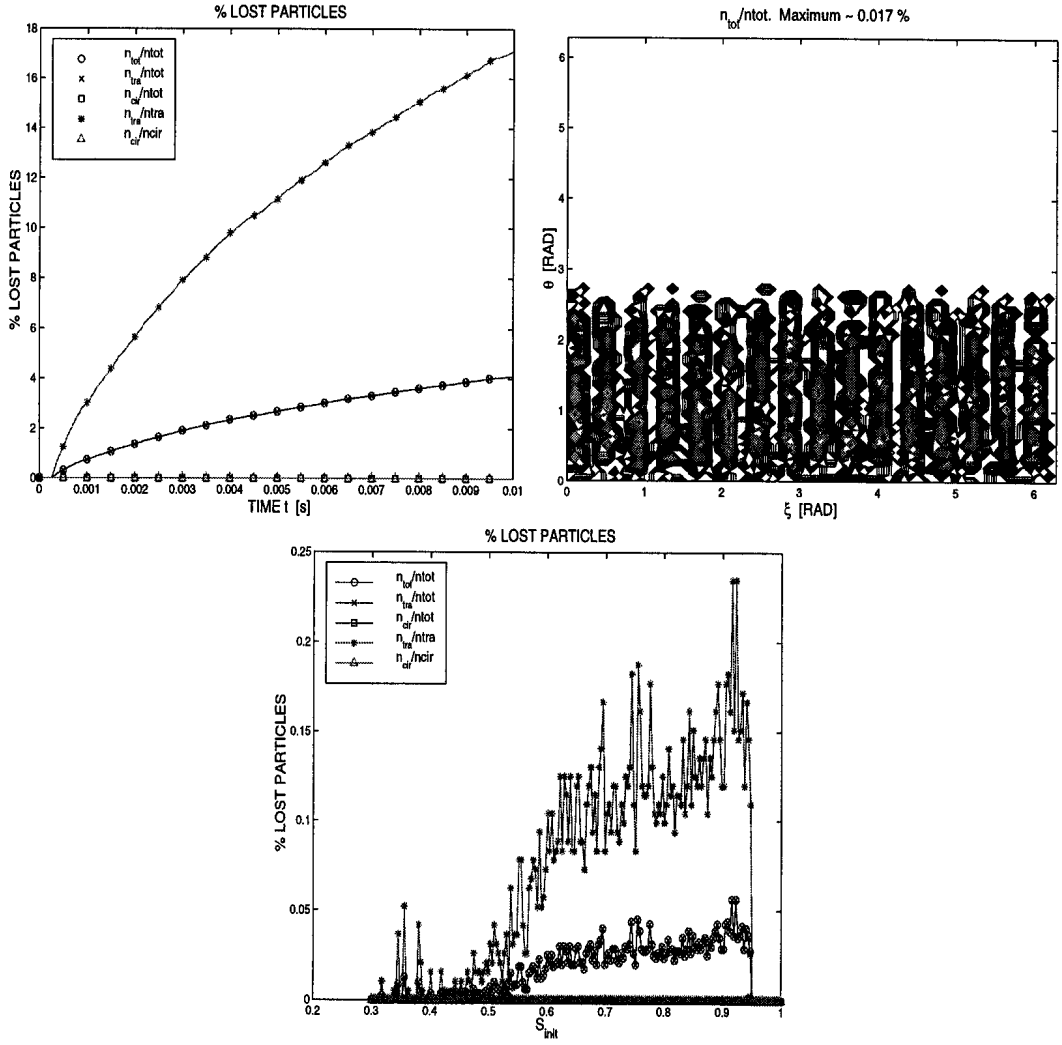
% LOST PARTICLES
n_tot/ntot
n_tra/ntot
n_cir/ntot
n_tra/ntra
n_cir/ncir
% LOST PARTICLES
TIME t [s]
n_tot/ntot. Maximum ~ 0.017 %
θ [RAD]
ξ [RAD]
% LOST PARTICLES
n_tot/ntot
n_tra/ntot
n_cir/ntot
n_tra/ntra
n_cir/ncir
% LOST PARTICLES
S_init

Figure 3:

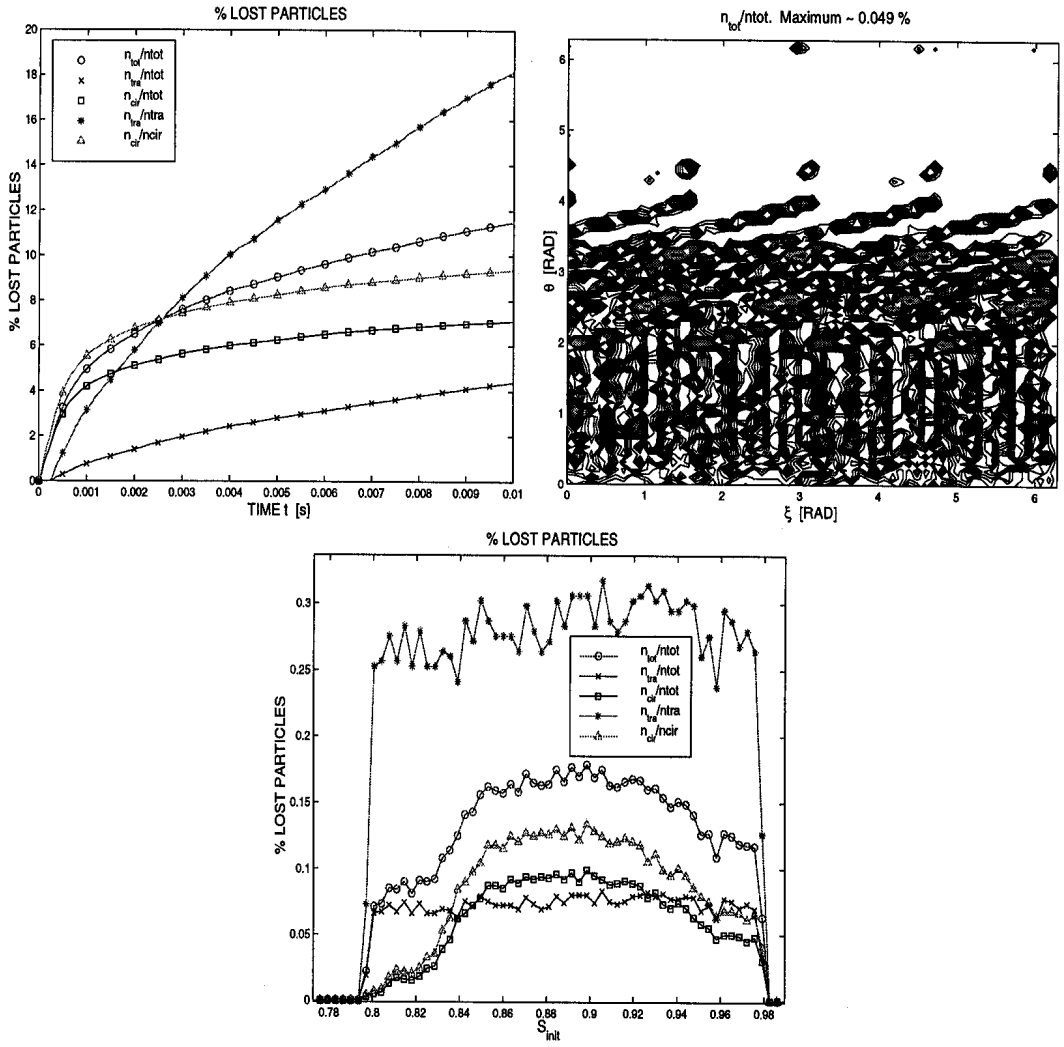
% LOST PARTICLES
n_tot/ntot
n_tra/ntot
n_cir/ntot
n_tra/ntra
n_cir/ncir
% LOST PARTICLES
TIME t [s]
n_tot/ntot. Maximum ~ 0.049 %
θ [RAD]
ξ [RAD]
% LOST PARTICLES
n_tot/ntot
n_tra/ntot
n_cir/ntot
n_tra/ntra
n_cir/ncir
% LOST PARTICLES
S_init

Figure 4:

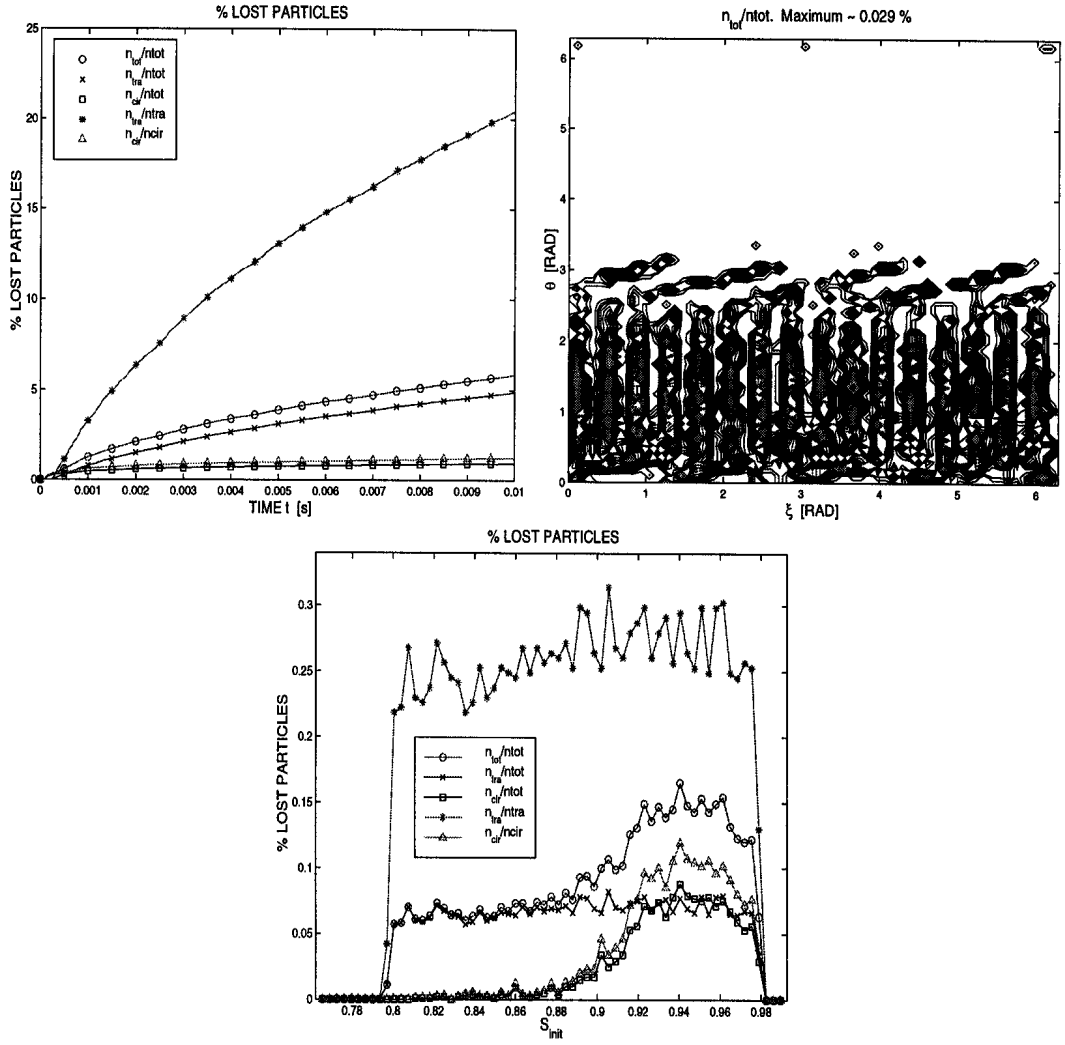
% LOST PARTICLES
% LOST PARTICLES
TIME t [s]
n_tot/ntot
n_tra/ntot
n_cir/ntot
n_tra/ntra
n_cir/ncir
n_tot/ntot. Maximum ~ 0.029 %
θ [RAD]
ξ [RAD]
% LOST PARTICLES
% LOST PARTICLES
S_init
n_tot/ntot
n_tra/ntot
n_cir/ntot
n_tra/ntra
n_cir/ncir

Figure 5: